

# An optimized scheme for detecting magneto-optic effects in ultrathin films with Sagnac interferometry

Cite as: Rev. Sci. Instrum. **93**, 093101 (2022); <https://doi.org/10.1063/5.0090061>

Submitted: 02 March 2022 • Accepted: 15 August 2022 • Published Online: 15 September 2022

 X. D. Zhu, E. K. Ko,  G. Kimbell, et al.





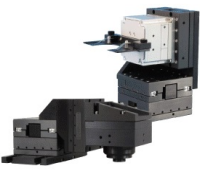
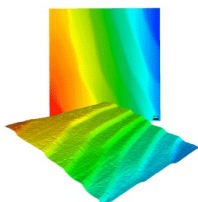
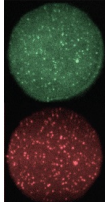
View Online



Export Citation



CrossMark

	<p>Nanopositioning Systems</p> 	<p>Modular Motion Control</p> 	<p>AFM and NSOM Instruments</p> 	<p>Single Molecule Microscopes</p> 
---	--	--	---	--

# An optimized scheme for detecting magneto-optic effects in ultrathin films with Sagnac interferometry

Cite as: Rev. Sci. Instrum. 93, 093101 (2022); doi: 10.1063/5.0090061

Submitted: 2 March 2022 • Accepted: 15 August 2022 •

Published Online: 15 September 2022



View Online



Export Citation



CrossMark

X. D. Zhu,<sup>1,2,a)</sup>  E. K. Ko,<sup>3,4</sup> G. Kimbell,<sup>5</sup>  and J. Robinson<sup>5</sup> 

## AFFILIATIONS

<sup>1</sup> Department of Physics and Astronomy, University of California, Davis, California 95616, USA

<sup>2</sup> Department of Optical Sciences and Engineering, Fudan University, Shanghai 200045, China

<sup>3</sup> Center for Correlated Electron Systems, Institute for Basic Science (IBS), Seoul 08826, Republic of Korea

<sup>4</sup> Department of Physics and Astronomy, Seoul National University, Seoul 08826, Republic of Korea

<sup>5</sup> Department of Materials Science and Metallurgy, University of Cambridge, Cambridge CB3 0FS, United Kingdom

<sup>a)</sup> Author to whom correspondence should be addressed: [xdzhu@physics.ucdavis.edu](mailto:xdzhu@physics.ucdavis.edu)

## ABSTRACT

Sagnac interferometry is advantageous in measuring time-reversal-symmetry breaking effects in ferromagnetic and antiferromagnetic materials as it suppresses time-reversal symmetric birefringent effects that are ubiquitous and often overwhelming in optical detection systems. When its sensitivity is limited only by the amplifier noise in the photo-detector, one needs to optimize the optical power that returns to the detector. We demonstrate an experimental scheme that maximizes the returning optical power in a Sagnac interferometry when detecting the magneto-optic effect in ultrathin films. In this scheme, the optical beam bearing the Faraday effect on a thin film is reflected at a second surface coated with a highly reflective gold film. The gold film increases the returned optical power by a factor of 4–5. For a normal-incidence Sagnac interferometer, this scheme yields an increase in the signal-to-noise ratio by the same factor. For an oblique-incidence Sagnac interferometer, this scheme should yield an increase in the signal-to-noise ratio by a factor of 20–25. For illustration, this scheme is used to measure magnetization curves and Kerr rotation images of 4.5-unit-cell thick SrRuO<sub>3</sub>(001) grown on SrTiO<sub>3</sub>(001).

Published under an exclusive license by AIP Publishing. <https://doi.org/10.1063/5.0090061>

## I. INTRODUCTION

Non-reciprocal optical responses or magneto-optic effects in solids are among the most extensively studied characteristics of ferromagnetic materials and materials with other forms of broken time-reversal symmetry.<sup>1–5</sup> The main advantages in optical detection of magnetism derive from its being a local probe in the time domain,<sup>6</sup> frequency domain,<sup>3</sup> spatial domain,<sup>7,8</sup> and symmetry domain.<sup>3,9</sup> Such a local probe enables time-resolved characterization, resonance enhancement, spatial mapping, and probing magnetism while suppressing much larger non-magnetic effects. The latter is realized in Sagnac interferometry,<sup>10</sup> particularly zero-loop-area Sagnac interferometry, in which the time-reversal symmetry breaking effect arising from the Earth's rotation is removed.<sup>11,12</sup> Since the early report by Spielman *et al.*,<sup>10</sup> Sagnac interferometry has

been broadly used in studies of ferromagnetic materials and time-reversal symmetry breaking effects in unconventional superconductors.<sup>4,12–16</sup> Magneto-optic (MO) effects in non-ferromagnetic materials are weak and often yield a Kerr rotation in the range 10<sup>−8</sup>–10<sup>−6</sup> radians.<sup>4,13,14</sup> Without external modulation,<sup>6,8</sup> Sagnac interferometry is presently the most sensitive probe to MO effects in these materials.

The sensitivity of a Sagnac interferometer is ultimately limited by a combination of the optical power that returns to the photo-detector,<sup>11,17</sup>  $P_{\text{det}}$  (in unit of Watt), and the noise equivalent power of the detector, NEP, in unit of W Hz<sup>−0.5</sup>. The sensitivity can then be defined as  $S \equiv 2(\text{NEP}/P_{\text{det}})$ , in unit of radian Hz<sup>−0.5</sup>. The factor of 2 introduced here is to account for the fact that the MO effect is contained in the first-order time-modulated portion (~50%) of optical power at the detector. When the NEP of the detector is given, the smallest detectable MO effect is improved by reducing the noise

bandwidth or maximizing the optical power at the detector. In this work, we focus on the latter.

In a zero-loop-area Sagnac interferometer, the illuminating optical beam is reflected off a sample surface once at normal incidence or twice at oblique-incidence.<sup>12,16,18</sup> A normal-incidence Sagnac interferometer (NI-SI) detects polar MO effects.<sup>11</sup> An oblique-incidence Sagnac interferometer (OI-SI) detects longitudinal, transverse as well as polar MO effects.<sup>12</sup> The optical power at the detector is proportional to the reflectance of the sample in NI-SI or the square of the reflectance in OI-SI. The reflectance can vary by one order of magnitude, depending upon the optical dielectric constant of the sample. In practice, the low reflectance of a sample limits the sensitivity of a Sagnac interferometer. This is particularly severe for an oblique-incidence Sagnac interferometer when the optical beam reflects twice from the sample.

In this report, we describe an experimental scheme that improves the optical power at the detector that bears the magneto-optic effect from an ultrathin film sample on a substrate. For illustration, we present a study of the magneto-optic effect in a 1.77 nm-thick SrRuO<sub>3</sub>(001) film epitaxially grown on a non-magnetic SrTiO<sub>3</sub>(001) substrate in which a five-fold gain in the optical power at the detector is achieved. This means that such a scheme can improve the sensitivity of an oblique-incidence Sagnac interferometer by more than a factor of 20.

## II. FARADAY AND KERR ROTATION FROM AN ULTRATHIN FILM ON A TRANSPARENT SUBSTRATE AND DETECTION WITH SAGNAC INTERFEROMETERS

For a weakly absorbing bulk sample, the Kerr rotation in reflection comes from the imaginary part of the Voigt parameter  $Q \equiv Q' + iQ''$ , while the Faraday rotation in transmission comes from the real part of  $Q$ .<sup>1,16,19</sup> For a thin film sample on a transparent substrate, the Kerr rotation and Faraday rotation both come from the real part of  $Q$  in the film and thus measure the same magneto-optic effect.<sup>19</sup> By detecting the Faraday rotation in transmission instead of the Kerr rotation in reflection from the same film, the optical power at the detector can be significantly enhanced. This is because the transmitted beam bearing the Faraday effect can be reflected with a second surface of high reflectance and sent back to the detector. A similar use of a highly reflective metal layer to enhance the optical reflection for Faraday effect detection of magnetic flux in high-temperature superconductors was reported by Jooss *et al.*<sup>20</sup>

In Fig. 1, we show a normal-incidence Sagnac interferometric scanning microscope in two modes: one is the Faraday mode that detects the reflection from the rear surface, the other is the Kerr mode that detects the reflection from the front surface.

We study the magneto-optic effect in a (001)-oriented ultrathin film of SrRuO<sub>3</sub> magnetized along the (001) axis. The film is epitaxially grown on a transparent SrTiO<sub>3</sub>(001) substrate and has a thickness of  $d = 1.77$  nm. The effect from the film on optical reflection and transmission can be treated as a surface-bound perturbation. Let  $\epsilon_{STO}$  be the optical dielectric constant of the SrTiO<sub>3</sub>(001) substrate. At optical wavelength  $\lambda = 0.78 \mu\text{m}$ ,  $\epsilon_{STO} = 5.3$  and is real. Let  $\epsilon_{SRO}$  be the optical dielectric constant of SrRuO<sub>3</sub>. At  $\lambda = 0.78 \mu\text{m}$ , it has a significant imaginary part as well as a real part.<sup>21–23</sup> We define

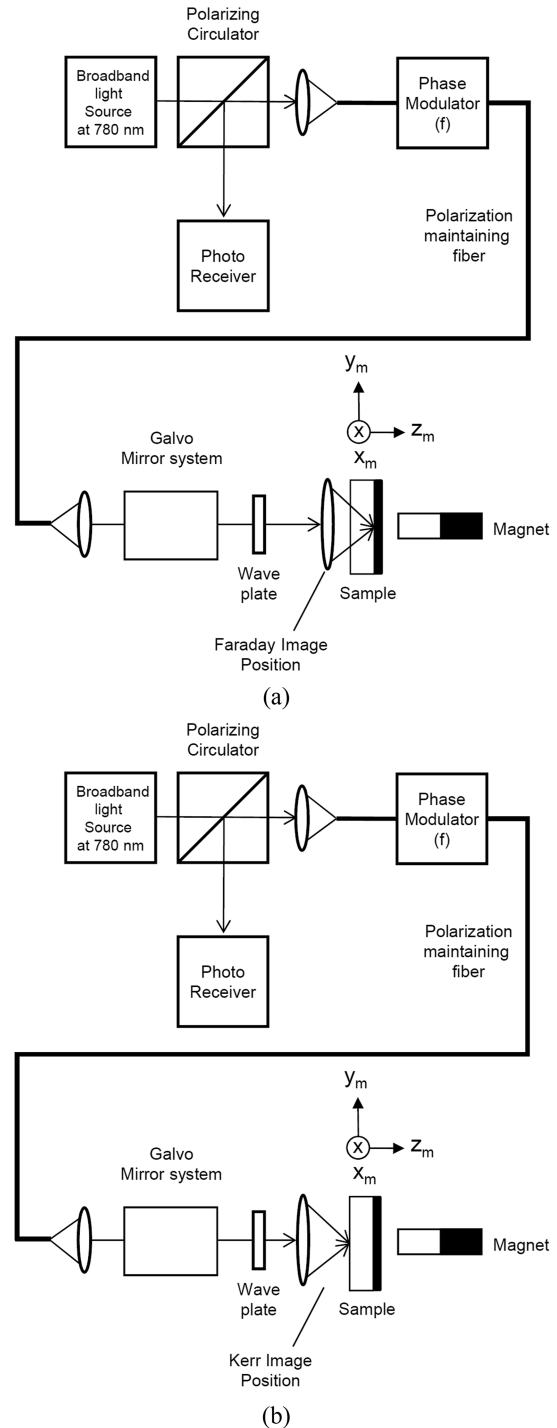


**FIG. 1.** (a) A normal-incidence zero-area Sagnac interferometric scanning microscope in Faraday mode for detecting Faraday rotation through the sample when the illumination beam is focused on the rear surface and reflected back. (b) The normal-incidence zero-area Sagnac interferometric scanning microscope in Kerr mode for detecting Kerr rotation when the illumination beam is focused on the front surface and reflected back. The lens immediately after the polarization-maintaining fiber focused the reflected beam back into the fiber to complete the Sagnac loop.

$\delta\epsilon = \epsilon_{SRO} - \epsilon_{STO}$ . The dielectric tensor  $\vec{\epsilon}$  as a function of  $z$  from the surface into the sample consisting of the film and the substrate is given by<sup>19</sup>

$$\vec{\epsilon} = \begin{pmatrix} \epsilon_{STO} & 0 & 0 \\ 0 & \epsilon_{STO} & 0 \\ 0 & 0 & \epsilon_{STO} \end{pmatrix} + d\delta(z) \begin{pmatrix} \delta\epsilon & -iQm_z & 0 \\ iQm_z & \delta\epsilon & 0 \\ 0 & 0 & \delta\epsilon \end{pmatrix}. \quad (1)$$

Since the film thickness  $d = 1.77$  nm is much smaller than the optical wavelength  $\lambda$ , the diagonal elements of the tensor associated with the film have a negligible effect on the reflection matrix and transmission matrix. The off-diagonal elements of the tensor associated with the film introduce the first-order magneto-optic effect on reflection and transmission.<sup>19</sup> Following the treatment described by Zhu,<sup>19</sup> the reflection matrix due to reflection from the front surface of the sample is given by<sup>24</sup>

$$\mathbb{R}_s = \begin{pmatrix} -\left(\frac{\sqrt{\epsilon_{STO}} - 1}{\sqrt{\epsilon_{STO}} + 1}\right) & \frac{4\pi d}{\lambda} \frac{Qm_z}{(\sqrt{\epsilon_{STO}} + 1)^2} \\ -\frac{4\pi d}{\lambda} \frac{Qm_z}{(\sqrt{\epsilon_{STO}} + 1)^2} & -\left(\frac{\sqrt{\epsilon_{STO}} - 1}{\sqrt{\epsilon_{STO}} + 1}\right) \end{pmatrix} \equiv \begin{pmatrix} r_n & \Delta_s \\ -\Delta_s & r_n \end{pmatrix}. \quad (2)$$

The Kerr rotation from the film is given by

$$\theta_{K,\text{film}} = \text{Re}\left\{\frac{\Delta_s}{r_n}\right\} = -\text{Re}\left\{\frac{4\pi d}{\lambda} \frac{Q}{\epsilon_{STO} - 1}\right\} m_z. \quad (3)$$

For the Faraday effect, we reflect the transmitted beam off a second surface with high reflectance  $R_2 \sim 1$ . This beam passes through the film once again and emerges as another reflected beam. The net transmission matrix for this beam can be regarded as an effective "reflection" matrix as follows:

$$\mathbb{R}_{s,\text{eff}} = \frac{4\sqrt{R_2}\sqrt{\epsilon_{STO}}}{(\sqrt{\epsilon_{STO}} + 1)^2} \begin{pmatrix} 1 & \frac{4\pi d Qm_z}{\lambda(\sqrt{\epsilon_{STO}} + 1)} \\ -\frac{4\pi d Qm_z}{\lambda(\sqrt{\epsilon_{STO}} + 1)} & 1 \end{pmatrix}. \quad (4)$$

The net Faraday rotation is given by

$$\Theta_{F,\text{film}} = \text{Re}\left\{\frac{4\pi d}{\lambda} \frac{Q}{\sqrt{\epsilon_{STO}} + 1}\right\} m_z. \quad (5)$$

At the detector, the optical power associated with the Faraday rotation is proportional to  $(4\sqrt{R_2}\epsilon_{STO}/(\sqrt{\epsilon_{STO}} + 1)^2)^2$ . Compared to the optical power associated with the Kerr rotation,  $(\sqrt{\epsilon_{STO}} - 1)^2/(\sqrt{\epsilon_{STO}} + 1)^2$ , it is a factor of  $\gamma_1 = 16R_2\epsilon_{STO}/(\epsilon_{STO} - 1)^2$  larger. Let  $\sqrt{\epsilon_{STO}} = 2.3$ ,  $R_2 = 0.95$ , this factor is 4.4. Comparing Eq. (5) with Eq. (3), the Faraday rotation is still larger than the Kerr rotation by a factor of  $\gamma_2 = \sqrt{\epsilon_{STO}} - 1 = 1.3$ . Thus the overall enhancement is

$$\gamma = \gamma_1\gamma_2 = 16R_2\epsilon_{STO}(\sqrt{\epsilon_{STO}} - 1)/(\epsilon_{STO} - 1)^2 = 5.7, \quad (6)$$

$\gamma$  is the factor by which the optical power at the detector is enhanced by detecting the Faraday rotation instead of Kerr rotation. Next, we demonstrate this enhancement experimentally. It is noteworthy that using the same Sagnac interferometric microscope for detection, Kerr rotation and Faraday rotation for same  $m_z$  have opposite signs as shown in Eqs. (3) and (5). This is also confirmed experimentally.

### III. MATERIALS AND METHODS

For sample, we grow a 1.77 nm thick (4.5 unit cells) SrRuO<sub>3</sub>(001) film on a 0.5 mm thick SrTiO<sub>3</sub>(001) substrate.<sup>25</sup> The substrate is treated with buffered hydrofluoric acid to have a TiO<sub>2</sub>-termination and then annealed at 1000 °C for 3 h in ambient atmosphere. The SrRuO<sub>3</sub>(001) film is grown on the substrate using pulsed laser deposition with a KrF Excimer laser ( $\lambda = 0.248$   $\mu\text{m}$ ). The growth temperature is 700 °C and the oxygen ambient is 100 mTorr. The laser repetition rate is 2 Hz, and the single pulse energy per unit area is 2 J/cm<sup>2</sup>. We use polycrystalline SrRuO<sub>3</sub> as a target. The thickness is controlled by monitoring reflection high-energy electron diffraction patterns. The thickness is controlled so that regions of 4 u.c. (1.57 nm) and 5 u.c. (1.96 nm) have equal portions, yielding an average thickness of 4.5 u.c.<sup>25,26</sup> For such ultrathin SrRuO<sub>3</sub> films, the magnetic easy axis is nearly perpendicular to the film along the  $z$ -axis.<sup>27-29</sup> The quality of the film is confirmed by atomic force microscopy. After deposition, the backside of the substrate is polished with diamond lapping sheets (1  $\mu\text{m}$ -grit) and then coated with a 200 nm-thick gold film using  $e$ -beam evaporation. The normal-incidence reflectance from the coated back surface is  $R_{\text{Au}} = 0.95$ . The reflectance of the front surface covered with the ultrathin film is in essence that of a bare SrTiO<sub>3</sub>(001) substrate, namely,  $R_{\text{STO}} = (\sqrt{\epsilon_{STO}} - 1)^2/(\sqrt{\epsilon_{STO}} + 1)^2 = 0.16$ , using  $\sqrt{\epsilon_{STO}} = 2.3$  at  $\lambda = 0.78$   $\mu\text{m}$ .

The Sagnac interferometric microscope<sup>15</sup> is illustrated in Fig. 1. A polarized super-luminescence laser diode with a central wavelength  $\lambda = 780$  nm and a FWHM bandwidth of 50 nm (Superlum, Carrigtwohill, Ireland) is used as the illumination source. After collimation, the p-polarized beam passes through a polarizing circulator and is then focused with a 20 $\times$  objective lens into a polarization-maintaining (PM) fiber with the slow axis (SA) parallel to the p-polarization. At the other end of the PM fiber, the beam is coupled to an electro-optic phase modulator (EOM) with the SA of the fiber bisecting the TE and TM axes of EOM. The polarization components along the TE and TM axes form the two optical beams in the Sagnac interferometer. They pass through the Sagnac loop that follows in opposite directions. The difference in the phase accumulated by these two beams is measured with a phase-sensitive detection system. The Sagnac loop consists of a 10 m PM fiber with the SA and FA aligned parallel to the TE and TM axes of EOM. After emerging from the 10 m PM fiber, the beams pass through a galvo-mirror system and a quarter-wave-plate (QWP), and are then focused onto the sample with a 10 $\times$  objective lens. The slow axis of the QWP is set at a 45° angle from the SA of the 10 m PM fiber. After reflection from the sample, the beams return to the 10 m PM fiber to complete the Sagnac loop.<sup>12</sup> The microscope can be operated in Kerr mode or Faraday mode by setting the focal point of the beam at the front surface or the back surface. A negligible fraction of the reflection from the other surface makes it back into the fiber.

To acquire a Kerr rotation or a Faraday rotation image, the beams are scanned over a 340  $\times$  340  $\mu\text{m}^2$  area at a step size of 0.85  $\mu\text{m}$  in both directions. This is accomplished with an encoded galvo mirror assembly mounted on a stepper-motor controlled backlash-free rotation stage. The galvo mirror deflects the beam in the vertical plane, thus changing the pitch angle  $\theta_p$  of the beam; the rotation stage rotates the galvo mirror assembly in the horizontal plane, thus changing the yaw angle  $\phi_x$  of the beam. By stepping the pitch angle at increment  $\delta\theta_p = 0.00125^\circ$ , we scan the beam on

the focal plane by  $\delta y = 0.85 \mu\text{m}$ ; and by stepping the yaw angle at increment of  $\delta\phi_x = 0.0025^\circ$ , we move the beam on the focal plane by  $\delta x = 0.85 \mu\text{m}$ . The time constant at each pixel (a pair of  $x$  and  $y$  positions) is 0.03 s or 30 ms.

Magnetization curves of the sample during field-cooling and field-warming are measured between 140 and 30 K. The Curie temperature is  $\sim 120$  K. We measure the Kerr or Faraday rotation at ten vertical positions (i.e., ten yaw angles) with a fixed horizontal position.

The super-luminescence laser diode has an output power of 10 mW. When the beam is focused on the front surface of the SrTiO<sub>3</sub>(001) substrate where the 1.77 nm SrRuO<sub>3</sub>(001) film is deposited, the returned optical power at the photo-detector is 5.6  $\mu\text{W}$ . When the beam is focused on the rear surface of the SrTiO<sub>3</sub>(001) substrate where a 200 nm gold film is deposited, the returned optical power increases to 22  $\mu\text{W}$ , by a factor of  $\gamma_{1m} = 3.9$ , very close to the expected value  $\gamma_1 = 4.4$ . The dominant losses come from (1) passage through a fiber-coupled EOSPACE electro-optic phase modulator (EOM) with single-pass insertion loss of 50%; (2) reflection at surfaces of near-infrared AR-coated optical elements that form the polarizing circulator and at surfaces of two visible AR-coated objectives (a factor of 3 for single pass); (3) insertion loss when the free-space beam is coupled into PM fibers and from the PM-fiber of the EOM to the 10 m PM fiber (a factor of 2 for single pass); and (4) reflection at the sample (a factor of  $1/R_{STO} = 6.5$  at the front surface). If two visible AR-coated objectives are replaced by near infrared AR-coated objectives (for a much higher cost), the single-pass loss factor is improved only by a small factor 1.3.

#### IV. RESULTS

In Fig. 2, we show a Kerr rotation image of the 1.77 nm SrRuO<sub>3</sub>(001) film and the reflectance image of the front surface over an area of  $340 \times 340 \mu\text{m}^2$ . It is acquired after the sample is field-cooled from  $T = 140$  to 80 K in an external field of  $H_z = 97$  Oe applied along the surface normal. This field is sufficient to saturate the magnetization of the film. The dark lines are features that result from shallow scratches on the film. Since the film is first grown on the front surface of the substrate and then a 200 nm gold coating is deposited *ex situ* on the other side of the substrate, we expect scratch damages to the film. Depths of these scratches correspond to 1–3 unit cells removed from the film. Such a small removed thickness is not observable in the reflectance image. In the uniform region of the Kerr rotation image, the value of  $\theta_{K,\text{film}}$  is  $195 \pm 13 \mu\text{rad}$ . Using a similar normal-incidence Sagnac interferometer that is operated at optical wavelength of 1.55  $\mu\text{m}$ , Xia *et al.* reported a  $\theta_{K,\text{film}}$  of 156  $\mu\text{rad}$  from a 4-unit-cell-thick SrRuO<sub>3</sub>(001) film on an SrTiO<sub>3</sub>(001) substrate at 80 K.<sup>29</sup> In Fig. 3, we show the Faraday rotation image and the reflectance image from the gold-coated surface over the same area of the SrRuO<sub>3</sub>(001) film. The sign of the measured Faraday rotation is opposite to that of the Kerr rotation as we should expect from Eqs. (3) and (5). The negative of the measured Faraday rotation is shown in the figure. The sharp lines in the Kerr image are blurred and become shadows due to the fact that scratches on the SrRuO<sub>3</sub>(001) film are now illuminated by an unfocused beam. New sharp features in the Faraday rotation image are scratches on the gold-coated SrTiO<sub>3</sub> surface. The same features are present in the

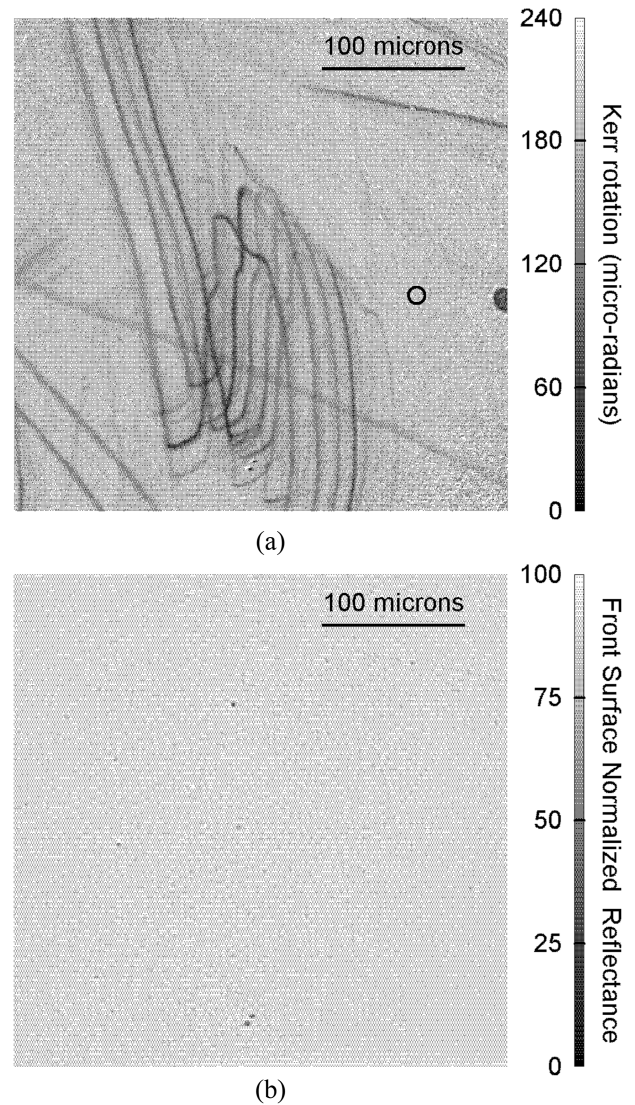


**FIG. 2.** (a) Kerr rotation angle from a 1.77 nm SrRuO<sub>3</sub>(001) film on SrTiO<sub>3</sub>(001) over an area of  $340 \times 340 \mu\text{m}^2$  after the sample is cooled from 140 to 80 K in an external field of  $H_z = 97$  Oe. The step size in both directions is 0.85  $\mu\text{m}$ . The open circle shows the position where the Kerr rotation as a function of temperature is measured. (b) Reflectance from the front surface of the sample over the same area. It is normalized by the maximum reflected optical power from the front surface.

reflectance image. In the uniform region of the Faraday rotation image, the average value of  $\Theta_{F,\text{film}}$  is  $247 \pm 15 \mu\text{rad}$ . It is a factor of  $\gamma_{2m} = 1.27$  larger than  $\theta_{K,\text{film}}$ , very close to the expected ratio  $\gamma_2 = \sqrt{\epsilon_{STO}} - 1 = 1.3$ . This means that the optical power at the detector is enhanced by a net factor of  $\gamma_m = \gamma_{1m}\gamma_{2m} = 5$ , close to our estimate of  $\gamma = 6$  from Eq. (6). The variations in Kerr rotation ( $\pm 13 \mu\text{rad}$ ) and Faraday rotation ( $\pm 15 \mu\text{rad}$ ) are due to the spatial variation of magnetization.

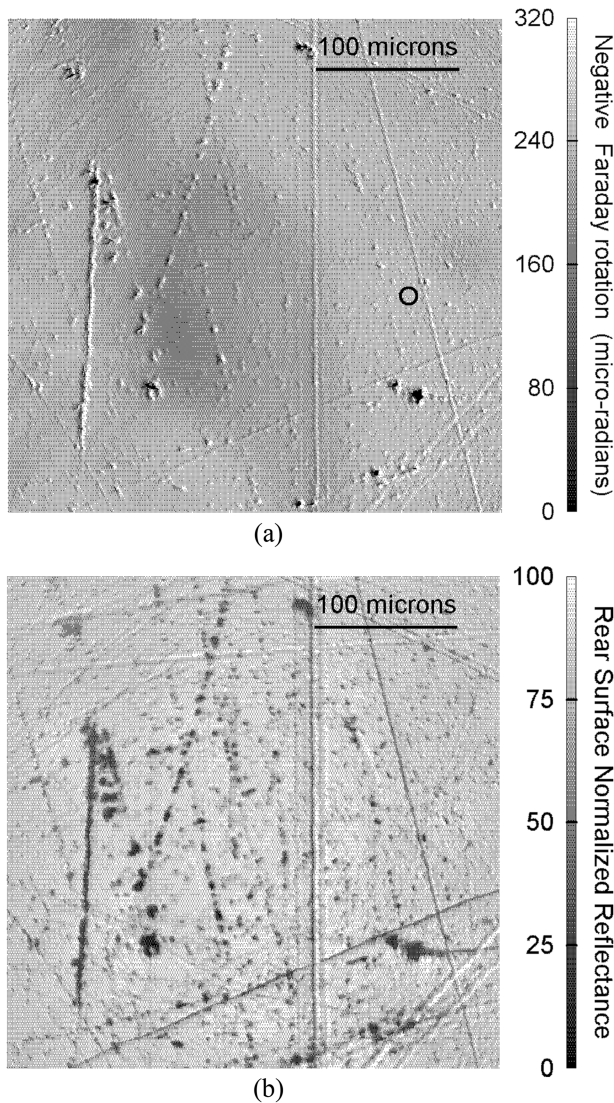


**FIG. 3.** (a) Faraday rotation angle from the same 1.77 nm SrRuO<sub>3</sub>(001) film on SrTiO<sub>3</sub>(001) over the same 340 × 340 μm<sup>2</sup> area. For the same magnetization in the film, the Faraday rotation angle is larger than the Kerr rotation angle by a factor of 1.27. The sharp features in the image are scratches on the second surface due to mechanical polishing. The dark shadow is due to the blurred magnetic features in the Kerr image in Fig. 2. The open circle shows the position where the Faraday rotation as a function of temperature is measured. (b) Reflectance over the same area, but from the rear surface of the sample with a 200 nm gold-coating. It is normalized by the maximum reflected optical power from the rear surface.

To further illustrate the improvement in signal-to-noise ratio for MO effect detection, we acquire magnetization curves in Kerr rotation and Faraday rotation. The curves are acquired from positions marked as open circles in Figs. 2 and 3. In Fig. 4, we show two magnetization curves: one from the Kerr rotation measurement; one from the Faraday rotation measurement. The time constants in both measurements are 0.3 s.  $\Theta_{F,\text{film}}$  is again larger than  $\theta_{K,\text{film}}$  by a factor of 1.27 as expected. The Faraday rotation curve is much

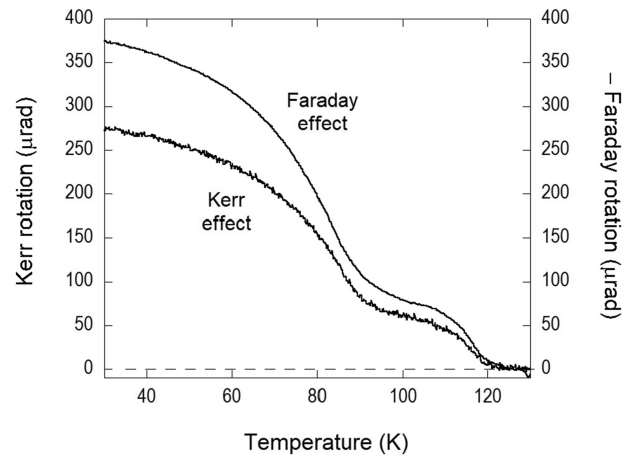


**FIG. 4.** Faraday rotation angle  $\Theta_{F,\text{film}}$  during field-cooling from 150 to 30 K and Kerr rotation angle  $\theta_{K,\text{film}}$  during field-warming from 30 to 150 K in an external field of  $H_z = 97$  Oe. The temperature-dependence of  $\Theta_{F,\text{film}}$  and  $\theta_{K,\text{film}}$  are nearly identical. The Faraday rotation angle is larger and much less noisier than the Kerr rotation angle.

less noisier than the corresponding Kerr rotation curve as a result of the improved signal-to-noise ratio. The magnetization curves show the presence of two transition temperatures,  $T_{C1} = 115$  K and  $T_{C2} = 80$  K. They are likely due to single unit cell thickness variations in the film.<sup>25,26</sup>

## V. DISCUSSION AND CONCLUSION

Sagnac interferometers have been used to detect minute signatures of magnetism and other time-reversal symmetry breaking effects in conventional and new quantum materials. With normal-incidence and oblique-incidence zero-area Sagnac interferometers, magneto-optic effects along any direction in a sample can be measured and analyzed. The sensitivity of a Sagnac interferometer is ultimately limited by the optical power at the photo-detector, particularly when the reflectance from a sample under study is low. A low sample reflectance is more problematic in oblique-incidence Sagnac interferometry when the illuminating beam is reflected twice from the sample to complete the Sagnac loop. We showed in this work that when detecting magneto-optic effects in ultrathin films on a substrate, the hurdle associated with a low sample reflectance can be removed by detecting the Faraday rotation instead. It is accomplished by returning the transmitted beam in full with a second highly reflective surface.

Using a 1.77 nm SrTiO<sub>3</sub>(001) film on a SrTiO<sub>3</sub>(001) substrate as an example, we demonstrated that one can recover nearly 100% of the transmitted beam and achieve a five-fold increase in optical power at the detector when detecting Faraday rotation instead of Kerr rotation for the same magneto-optic effect in the film. Such a five-fold optical power recovery is most significant in an oblique-incidence Sagnac interferometry. For example, instead of having the returned optical power to decrease further from 5.6 to 0.87 μW (recalling that the reflectance of a bare SrTiO<sub>3</sub> substrate at normal incidence  $R_{STO}$  is 0.16), the present scheme will

only reduce the returned power from 22 to 16  $\mu\text{W}$ . This should make oblique-incidence Sagnac interferometers equally sensitive as normal-incidence Sagnac interferometers.

By comparing Fig. 3 with Fig. 2, it would seem that the gain in signal-to-noise ratio by employing a second reflecting surface is at a huge expense of spatial resolution. This is because we intentionally use a 0.5 mm SrTiO<sub>3</sub>(001) substrate and an objective with  $f = 20$  mm so that the reflection from the front surface bearing the Kerr rotation effect and the reflection from the rear surface bearing the Faraday rotation effect can be separated for analysis. The loss in spatial resolution can be easily recovered by reducing the SrTiO<sub>3</sub>(001) substrate thickness from 0.5 mm to 50  $\mu\text{m}$  and using an objective with  $f = 75$  mm instead of  $f = 20$  mm.

As to the achievable detection limit of the present microscope, by replacing the current 10 mW light source with a 30 mW source, the optical power at the detector can be improved to 66  $\mu\text{W}$ , close to the maximally allowed power at a New Focus 1801 photo-detector employed in this microscope. The microscope should have the highest sensitivity allowed by the photo-detector. With  $NEP = 3.3 \times 10^{-12}$  W Hz<sup>-0.5</sup> for a New Focus 1801 photo-detector, an optical power of  $P_{\text{det}} = 66 \mu\text{W}$  at the detector translates into a detector-limited sensitivity of  $S = 2NEP/P_{\text{det}} = 10^{-7}$  radian Hz<sup>-0.5</sup>.

## ACKNOWLEDGMENTS

X.D.Z. acknowledges a Lecture Professorship from Fudan University in support of this work and the UCD Physics Liquid Helium Laboratory fund. E.K.K. acknowledges the major support provided by the Research Center Program of Korea Basic Science Institute (Grant No. IBS-R009-D1). G.K. was supported by the EPSRC through the Core-to-Core International Network “Oxide Superspin” (Grant No. EP/P026311/1) and the Doctoral Training Partnership Grant (Grant No. EP/N509620/1).

## AUTHOR DECLARATIONS

### Conflict of Interest

The authors have no conflicts to disclose.

## Author Contributions

**X. D. Zhu:** Conceptualization (lead); Formal analysis (lead); Investigation (lead); Methodology (lead). **E. K. Ko:** Data curation (supporting); Formal analysis (supporting); Funding acquisition (supporting); Methodology (supporting). **G. Kimbell:** Conceptualization (supporting); Formal analysis (supporting); Funding acquisition (supporting); Writing – review & editing (supporting). **J. Robinson:** Funding acquisition (supporting); Resources (supporting); Supervision (supporting); Writing – review & editing (supporting).

## DATA AVAILABILITY

The data that support the findings of this study are available from the corresponding author upon reasonable request.

## REFERENCES

- 1 Z. Q. Qiu and S. D. Bader, “Surface magneto-optic Kerr effect,” *Rev. Sci. Instrum.* **71**, 1243 (2000).
- 2 R. V. Pisarev, B. B. Krichevstov, and V. V. Pavlov, “Optical study of the antiferromagnetic-paramagnetic phase transition in chromium oxide Cr<sub>2</sub>O<sub>3</sub>,” *Phase Transitions* **37**, 63 (1991).
- 3 M. Fiebig, D. Fröhlich, B. B. Krichevstov, and R. V. Pisarev, “Second harmonic generation and magnetic-dipole-electric-dipole interference in antiferromagnetic Cr<sub>2</sub>O<sub>3</sub>,” *Phys. Rev. Lett.* **73**, 2127 (1994).
- 4 E. R. Schemm, W. J. Gannon, C. M. Wishne, W. P. Halperin, and A. Kapitulnik, “Observation of broken time-reversal symmetry in the heavy-fermion superconductor UPt<sub>3</sub>,” *Science* **345**, 190 (2014).
- 5 Y. Kota and H. Imamura, “Narrowing of antiferromagnetic domain wall in corundum-type Cr<sub>2</sub>O<sub>3</sub> by lattice strain,” *Appl. Phys. Express* **10**, 013002 (2017).
- 6 S. A. Crooker, D. D. Awschalom, and N. Samarth, “Time-resolved Faraday rotation spectroscopy of spin dynamics in digital magnetic heterostructures,” *IEEE J. Sel. Top. Quantum Electron.* **1**, 1082 (1995).
- 7 J. McCord, “Progress in magnetic domain observation by advanced magneto-optical microscopy,” *J. Phys. D: Appl. Phys.* **48**, 333001 (2015).
- 8 Y. K. Kato, R. C. Myers, A. C. Gossard, and D. D. Awschalom, “Observation of the spin Hall effect in semiconductors,” *Science* **306**, 1910 (2004).
- 9 M. Fiebig, D. Fröhlich, G. Sluyterman v. L., and R. V. Pisarev, “Domain topography of antiferromagnetic Cr<sub>2</sub>O<sub>3</sub> by second-harmonic generation,” *Appl. Phys. Lett.* **66**, 2906 (1995).
- 10 S. Spielman, J. S. Dodge, L. W. Lombardo, C. B. Eom, M. M. Fejer, T. H. Geballe, and A. Kapitulnik, “Measurement of the spontaneous polar Kerr effect in YBa<sub>2</sub>Cu<sub>3</sub>O<sub>7</sub> and Bi<sub>2</sub>Sr<sub>2</sub>CaCu<sub>2</sub>O<sub>8</sub>,” *Phys. Rev. Lett.* **68**, 3472 (1992).
- 11 J. Xia, P. T. Beyersdorf, M. M. Fejer, and A. Kapitulnik, “Modified Sagnac interferometer for high-sensitivity magneto-optic measurements at cryogenic temperatures,” *Appl. Phys. Lett.* **89**, 062508 (2006).
- 12 X. D. Zhu, “Symmetry consideration in zero loop-area Sagnac interferometry at oblique incidence for detecting magneto-optic Kerr effects,” *Rev. Sci. Instrum.* **88**, 083112 (2017).
- 13 H. Karapetyan, J. Xia, M. Hücker, G. Gu, J. Tranquada, M. Fejer, and A. Kapitulnik, “Evidence of chiral order in the charge-ordered phase of superconducting La<sub>1.87</sub>Ba<sub>0.125</sub>CuO<sub>4</sub> single crystals using polar Kerr-effect measurements,” *Phys. Rev. Lett.* **112**, 047003 (2014).
- 14 E. R. Schemm, R. E. Baumbach, P. H. Tobash, F. Ronning, E. D. Bauer, and A. Kapitulnik, “Evidence for broken time-reversal symmetry in the superconducting phase of URu<sub>2</sub>Si<sub>2</sub>,” *Phys. Rev. B* **91**, 140506 (2015).
- 15 X. D. Zhu, “Magnetic domains and unusual hysteresis loops of yttrium iron garnet crystals revealed by magneto-optic effect,” *AIP Adv.* **11**, 085214 (2021).
- 16 X. D. Zhu, R. Ullah, and V. Taufour, “Oblique-incidence Sagnac interferometric scanning microscope for studying magneto-optic effects of materials at low temperatures,” *Rev. Sci. Instrum.* **92**, 043706 (2021).
- 17 A. Fried, M. Fejer, and A. Kapitulnik, “A scanning, all-fiber Sagnac interferometer for high resolution magneto-optic measurements at 820 nm,” *Rev. Sci. Instrum.* **85**, 103707 (2014).
- 18 J. S. Dodge, L. Klein, M. M. Fejer, and A. Kapitulnik, “Symmetry of the magneto-optic response of the Sagnac interferometer,” *J. Appl. Phys.* **79**, 6186 (1996).
- 19 X. D. Zhu, “Linear optical responses beyond the electric dipole approximation on reflection and transmission: A perturbation treatment,” *OSA Continuum* **4**, 966 (2021).
- 20 C. Jooss, J. Albrecht, H. Kuhn, S. Leonhardt, and H. Kronmüller, “Magneto-optical studies of current distributions in high-T<sub>c</sub> superconductors,” *Rep. Prog. Phys.* **65**, 651 (2002).
- 21 H. S. Choi, J. Bak, J. S. Ahn, N. J. Hur, T. W. Noh, and J. H. Cho, “Determination of the optical constants of (Ca, Sr)RuO<sub>3</sub> films,” *J. Korean Phys. Soc.* **33**, 184 (1998).
- 22 J. S. Dodge, E. Kulatov, L. Klein, C. H. Ahn, J. W. Reiner, L. Miéville, T. H. Geballe, M. R. Beasley, A. Kapitulnik, H. Ohta, Y. Uspenski, and S. Halilov, “Temperature-dependent local exchange splitting in SrRuO<sub>3</sub>,” *Phys. Rev. B* **60**, R6987 (1999).

- <sup>23</sup>J. Lee, Y. Lee, T. Noh, K. Char, J. Park, S.-J. Oh, J.-H. Park, C. Eom, T. Takeda, and R. Kamo, "Optical investigation of the electronic structures of  $Y_2Ru_2O_7$ ,  $CaRuO_3$ ,  $SrRuO_3$ , and  $Bi_2Ru_2O_7$ ," *Phys. Rev. B* **64**, 245107 (2001).
- <sup>24</sup>X. D. Zhu and H. Zhang, "Hidden linear optical response reveals crystalline symmetry," *Opt. Lett.* **45**, 2439 (2020).
- <sup>25</sup>G. Kimbell, P. Sass, B. Woltjes, E. Ko, T. Noh, W. Wu, and J. Robinson, "Two-channel anomalous Hall effect in  $SrRuO_3$ ," *Phys. Rev. Mater.* **4**, 054414 (2020).
- <sup>26</sup>L. Wang, Q. Feng, H. G. Lee, E. K. Ko, Q. Lu, and T. W. Noh, "Controllable thickness inhomogeneity and Berry curvature engineering of anomalous Hall Effect in  $SrRuO_3$  ultrathin films," *Nano Lett.* **20**, 2468 (2020).
- <sup>27</sup>M. Schultz, S. Levy, J. W. Reiner, and L. Klein, "Magnetic and transport properties of epitaxial films of  $SrRuO_3$  in the ultrathin limit," *Phys. Rev. B* **79**, 125444 (2009).
- <sup>28</sup>E. K. Ko, J. Mun, H. G. Lee, J. Kim, J. Song, S. H. Chang, T. H. Kim, S. B. Chung, M. Kim, L. Wang, and T. W. Noh, "Oxygen vacancy engineering for highly tunable ferromagnetic properties: A case of  $SrRuO_3$  ultrathin film with a  $SrTiO_3$  capping layer," *Adv. Funct. Mater.* **30**, 2001486 (2020).
- <sup>29</sup>J. Xia, W. Siemons, G. Koster, M. R. Beasley, and A. Kapitulnik, "Critical thickness for itinerant ferromagnetism in ultrathin films of  $SrRuO_3$ ," *Phys. Rev. B* **79**, 140407(R) (2009).